Chemical Engineering Journal 167 (2011) 597–602

Contents lists available at ScienceDirect

Chemical Engineering Journal

journal homepage: www.elsevier.com/locate/cej

A million-channel CO-PrOx microreactor on a fingertip for fuel cell application

N.J. Divins[a,b], E. López[a,c], M. Roig[a], T. Trifonov[b,d], A. Rodríguez[d], F. González de Rivera[e], L.I. Rodríguez[e], M. Seco[e], O. Rossell[e], J. Llorca[a,b,*]

[a] Institut de Tècniques Energètiques, Universitat Politècnica de Catalunya, Diagonal 647, ed. ETSEIB, 08028 Barcelona, Spain
[b] Centre de Recerca en Nanoenginyeria, Universitat Politècnica de Catalunya, Pasqual i Vila 15, 08028 Barcelona, Spain
[c] Planta Piloto de Ingeniería Química (CONICET-UNS), Camino de la Carrindanga km7, 8000 Bahía Blanca, Argentina
[d] Departament d'Enginyeria Electrònica, Universitat Politècnica de Catalunya, Campus Nord, Mòdul C4, Jordi Girona 1-3, 08034 Barcelona, Spain
[e] Departament de Química Inorgànica, Universitat de Barcelona, Martí i Franquès 1-11, 08028 Barcelona, Spain

ARTICLE INFO

Keywords:
CO-PrOx
Microreactor
Macroporous silicon
Gold catalyst
Hydrogen purification
PEMFC

ABSTRACT

A silicon micromonolith containing ca. 40000 regular channels of 3.3 μm in diameter per square millimeter has been successfully functionalized with an Au/TiO_2 catalyst for CO preferential oxidation (CO-PrOx) in the presence of hydrogen. The functionalization of the silicon microchannels has been accomplished by growing a SiO_2 layer on the channel walls, followed by exchange with a titanium alkoxyde precursor and decomposition into TiO_2 and, finally, by anchoring carbosilanethiol dendron protected pre-formed Au nanoparticles. Catalytically active centers at the $Au–TiO_2$ interface have been obtained by thermal activation. With this method, an excellent homogeneity and adherence of the catalytic layer over the microchannels of the silicon micromonolith has been obtained, resulting in geometric exposed surface area values of about 4×10^5 m^2/m^3. The functionalized silicon micromonolith has been tested for CO-PrOx at 363–433 K and $\lambda = 2$ under $H_2/CO = 0–20$ (molar), and the results have been compared with those obtained over a conventional cordierite monolith with 400 cpsi loaded with the same catalyst. The performance of the silicon micromonolith, which converts ca. 1 NmL of CO per minute and mL of microreactor at 398 K under $H_2/CO \sim 20$, is two orders of magnitude higher than that of conventional monolithic structures, suggesting that silicon micromonoliths could be particularly effective for hydrogen purification in low-temperature microfuel cells for portable applications.

1. Introduction

Tendency towards miniaturization is a palpable reality in the field of power sources for portable electronic devices in general and in fuel cell systems in particular. Compact proton exchange membrane fuel cells (PEMFC) appear suitable for power generation in small-scale applications based on their high efficiency and favorable power-to-weight ratio. Hydrogen for the fuel cell feeding can be conveniently generated on-site and on-demand via reforming technologies. Nevertheless, carbon monoxide is always formed as a by-product during the reforming reactions and it is well known that only a few ppm of CO poisons the anode electrocatalysts of PEMFC. In this context, the suppression of CO from the reformer effluent appears mandatory. CO Preferential Oxidation (CO-PrOx) is particularly appealing when applied to low-scale/portable reformer-PEMFC systems due to its fairly simple implementation, low operation costs and minimal loss of hydrogen [1,2].

Although considerable work has been carried out on hydrogen production and subsequent purification using packed bed reactors, the scale reduction required for portable applications renders their utilization impractical. Moreover, hydrogen purification reactions show strong thermal effects and conventional fixed-bed reactors exhibit poor heat transfer characteristics. Microreactors assess both problems of moving down the scale and increasing the heat transfer rate by the deposition of the catalyst directly on the reactor walls. The introduction of new manufacture techniques permits, along with the miniaturization involved, the achievement of remarkable increases on the specific contact area. The small dimensions attained for the microchannels and their high reproducibility allow better reaction control by achieving previously inaccessible residence times and flow pattern homogeneity [3]. Microreactors appear as an invaluable technology for boosting the implementation of on-board generation of hydrogen for portable applications, thus avoiding limitations imposed by hydrogen storage [4]. Also, microreaction technology provides enhanced safe operation in the management of hydrogen-rich streams because large volumes are

* Corresponding author at: Institut de Tècniques Energètiques, Universitat Politècnica de Catalunya, Diagonal 647, ed. ETSEIB, 08028 Barcelona, Spain. Tel.: +34 934011708; fax: +34 934017149.
E-mail address: jordi.llorca@upc.edu (J. Llorca).

1385-8947/$ – see front matter © 2010 Elsevier B.V. All rights reserved.
doi:10.1016/j.cej.2010.07.072

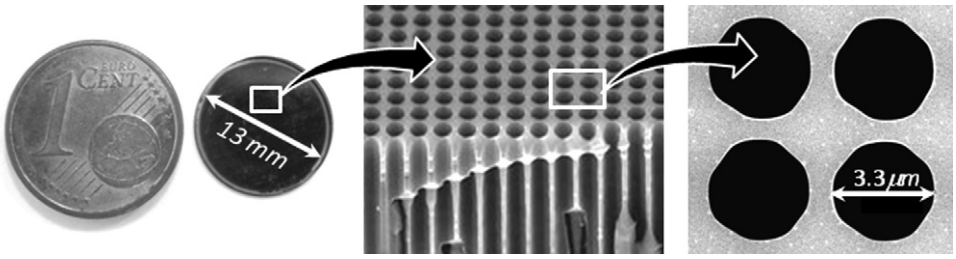

Fig. 1. Photograph of the silicon micromonolith used in this work compared to 1 cent of Euro and scanning electron microscopy images of the regularly arranged circular channels.

avoided, allowing the use of process parameters of otherwise explosive regimes.

However, the natural trend in miniaturization of fuel cell systems is followed with increasing difficulty by actual microreforming/micro-cleaning units. To further reduce the hydrogen generation scale while maintaining system efficiency is hardly attained using conventional geometries and/or manufacture techniques of actual microreactors. Therefore, the development of breakthrough technologies capable to provide higher hydrogen generation rates per unit volume and, at the same time, enable downscaling is required. In a pioneering publication by Llorca et al. [5], a new turn of the screw in miniaturization of systems for hydrogen production was accomplished using silicon micromonoliths with millions of regular and parallel microchannels per square centimeter with a diameter of only ~3–4 μm. Such geometry was achieved through photo-assisted electrochemical etching in a ~0.2-mm thick silicon wafer. The parallel channels, with a depth/diameter ratio >65, showed spectacular reproducibility and perfectly cylindrical shape, assuring excellent flow distribution. By means of a novel complexation–decomposition method, the channels walls were successfully coated with a homogeneous thin layer of cobalt catalyst for low-temperature steam reforming of ethanol (ESR). With the resultant geometry, the specific contact area increased with respect to conventional microreactors up to fabulous values of 10^5–10^6 m^2/m^3. A ~0.01 cm^3 unit comprising >10^6 channels was successfully tested for ESR under residence times <1 s, rendering specific production rates exceeding 50 NL of H_2 per mL of liquid fed and cm^3 of reactor [5,6]. The low-temperature reforming of ethanol offers a nice solution for supplying hydrogen to portable fuel cells due to its high volumetric energy density, low cost, safety, and easy transportation [7]. Recently, we have also reported hierarchical design concepts including several structures in-series based on silicon micromonoliths mounted in proper microreactor casings and provided with the necessary periphery for ESR [8].

In this work, we report on the use of silicon micromonoliths loaded with Au/TiO_2 catalyst for low-temperature CO-PrOx aimed at downstream hydrogen purification for PEMFC feeding. Gold nanoparticles deposited on oxide supports, such as TiO_2, are effective to selectively oxidize CO in hydrogen-rich environments [9]. Furthermore, CO oxidation is a kinetically rapid and exothermic reaction, so the ability of the reactor design to eliminate the heat of reaction from the reaction medium to maintain adequate selectivity levels (i.e. avoid H_2 losses and prevent the onset of the reverse gas-shift reaction) is of crucial importance. Taking advantage from the extremely high specific surface areas achieved by the silicon micromonolith geometry and the good conductivity of the Si matrix itself, isothermal operation is feasible along with appropriate reaction rates. The outstanding reproducibility achieved on both the support geometry and the catalyst deposition strongly prevents from formation of local hot spots.

2. Materials and methods

2.1. Catalyst and substrate preparation

Photoassisted electrochemical etching [10] was used to prepare silicon micromonoliths with straight, parallel channels of 3.3 μm in diameter over ⟨1 0 0⟩ *n*-type float-zone silicon. Experimental details have been already reported [5,8]. Briefly, silicon was first pre-structured by lithography and etched with hydrofluoric acid solution at a constant potential of 2 V. The backside was illuminated through an array of LEDs with an 880 nm peak emission wavelength and the channels were opened with tetramethylammonium hydroxide solution at 358 K. The resulting structures were silicon micromonoliths with a length of ca. 0.2 mm containing 4×10^6 cylindrical channels/cm^2 opened at both sides and arranged in a square lattice with a periodicity of 4 μm. Fig. 1 shows scanning electron microscopy images of the silicon micromonoliths exhibiting the regular array of cylindrical microchannels. The specific contact area is 3.5×10^5 m^2/m^3.

In this work, the micromonoliths were thermally treated at 1373 K under a dry O_2 atmosphere for 30 min to form a ca. 60-nm thick SiO_2 layer on the channel walls. The terminal hydroxyl groups of the SiO_2 layer were exchanged at room temperature with titanium isopropoxide (Panreac), which was forced to pass through the micromonolith channels by applying a pressure gradient of 75 kPa. A homogeneous and well-adhered layer of TiO_2 was obtained by thermal decomposition at 723 K for 4 h (1 K min^{-1}). Finally, preformed gold nanoparticles were grafted onto the TiO_2 support (2% w/w). This was accomplished by free impregnation by passing a toluene solution of the carbosilanethiol dendron protected gold nanoparticles through the silicon micromonolith channels coated with TiO_2 and calcination at 673 K for 2 h (2 K min^{-1}). For comparative purposes, conventional cordierite monoliths (2 cm length and 2 cm diameter) with square cross-section of side ca. 1.2 mm (400 cpsi, Corning Celcor®) were also coated with the Au/TiO_2 catalyst (2% w/w) following the same method. The gold nanoparticles were obtained by the known two phase transfer method [11]. In short, H[$AuCl_4$] from an aqueous phase was transferred to a toluene phase using tetraoctylammonium bromide as the phase transfer agent. Then, the acid was reduced by sodium borohydride in the presence of the thiol-functionalized dendron $HS(CH_2)_3Si((CH_2)_3Si(Me)_3)_3$, which prevents particles from aggregation [12]. It is worthy of note that the carbosilane dendron used in this work was designed and synthesized because of its specific dendritic structure able to difficult the potential intercalation of the monolayers from different nanoparticles and avoid, in turn, their approach. Thus, an appropriate distance among them was achieved and the potential aggregation of the gold nanoparticles in the impregnation of the toluene solution through the silicon micromonolith channels coated with TiO_2 was minimized.

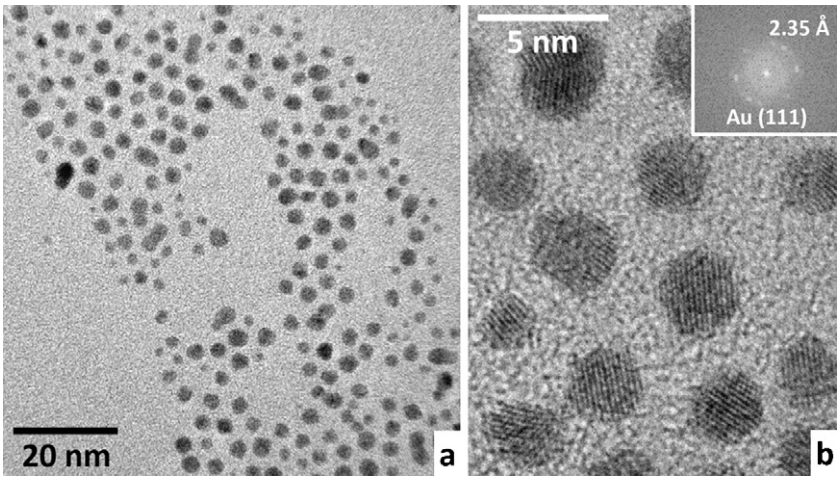

Fig. 2. (a) Transmission electron microscopy (TEM) image of dendrimer capped Au nanoparticles. (b) Detailed high resolution TEM image of several dendrimer capped Au nanoparticles and their corresponding Fourier Transform image.

2.2. Characterization techniques

High resolution transmission electron microscopy (HRTEM) was carried out using a JEOL JEM 2010F electron microscope equipped with a field emission source at an accelerating voltage of 200 kV. In the case of the solution with pre-formed Au nanoparticles, the sol was directly dropped onto a carbon-coated grid. For the Au/TiO_2 catalyst, powder was suspended in methanol for about 1 min under ultrasonic treatment before it was deposited on a holey carbon-coated grid. The microscope was calibrated at different magnifications before and after measurements using appropriate standards. The point-to-point resolution achieved was 0.19 nm and the resolution between lines was 0.14 nm. A minimum of 200 particles were measured in each sample for particle size determination. Scanning electron microscopy (SEM) was carried out on a Neon40 Crossbeam Station (Zeiss) equipped with a field emission (FE) SEM and focused ion beam (FIB). High resolution SEM pictures were taken after cleaving the sample at different depths along the channels to see the homogeneity of pore infiltration. In some cases, a FIB-cut (Ga^+, 30 keV) groove was made on the pore surface after previous e-beam assisted Pt deposition in order to estimate the thickness of deposited Au/TiO_2 layer. For surface analysis, X-ray photoelectron spectroscopy (XPS) was performed with a SPECS system equipped with an Al anode XR50 source operating at 150 W and a Phoibos MCD-9 detector. XP spectra were recorded with pass energy of 25 eV at 0.1 eV steps at a pressure below 10^{-9} mbar and binding energies were referred to the C 1 s signal. In situ thermal treatments were performed directly in the analysis chamber. X-ray diffraction (XRD) measurements were performed with a Siemens D5000X diffractometer with Cu Kα incident radiation. XRD profiles were recorded from 3° to 75° (2θ) at a step size of 0.02° and step time of 1 s.

2.3. Catalytic tests

For catalytic testing, a silicon micromonolith disk of 13 mm in diameter was cut with a laser device (Fig. 1) and glued with epoxy into a stainless steel washer (external diameter 19 mm, internal diameter 8 mm), which was subsequently sealed in a stainless steel housing inside a furnace (Carbolite, accuracy ±0.1 K). Reaction mixtures consisting of CO and air ($\lambda = 2$, see equation 1) and different concentrations of H_2 balanced in Ar were prepared using independent mass flow controllers (M + W Instruments). The feed was passed at atmospheric pressure through the silicon micromonolith at 5 STP mL min^{-1}, leading to a contact time of 0.09 s. Reaction products were analyzed continuously online with an Agilent 3000A gas micro-chromatograph equipped with MS 5 Å, PlotU, and Stabilwax columns. Conventional monoliths were tested under the same reactant mixtures at 10 STP mL min^{-1}, resulting in a contact time of 30 s.

$$\lambda = \frac{2 \cdot y^{+}_{O_2}}{y^{+}_{CO}} \quad (1)$$

3. Results and discussion

3.1. Catalyst deposition

Given the small dimensions of the channels in the silicon micromonoliths, the conventional and easiest way for depositing catalyst coatings over catalytic walls, the washcoating method, proved to be inadequate. For that reason, we developed a new method specifically designed for coating the microchannel walls with Au/TiO_2 catalyst, as detailed in Section 2.1. In order to facilitate the adherence of TiO_2 onto the silicon substrate, the silicon micromonoliths were first oxidized to develop a thin SiO_2 layer of about 60-nm thick. The hydroxyl groups attached to the surface of the oxide layer acted as anchoring sites and interacted with the alkoxyde precursor, $Ti(^{i}PrO)_4$, leading to the formation of a homogeneous TiO_2 layer upon calcination at 723 K. The synthesis was followed by X-ray diffraction (XRD) and scanning electron microscopy (SEM). Diffraction peaks at 25.3, 37.9, 48.1, 54.0 and 55.1° in the XRD profiles indicated the formation of the anatase polymorph of TiO_2.

When dispersed as fine particles of less than ~10 nm in dimension over selected metal oxides, gold exhibits exceptionally high activity in a variety of reactions, such as CO oxidation [13,14]. The mode of operation of Au–Ti–O catalysts for this reaction remains unclear, but the roles of the support, the Au particle size, and the periphery between the support and the Au particles have been recognized. In particular, the anatase form of TiO_2 enhances CO oxidation. As regards the Au particle size, there is strong particle size dependence and mainly small nanoparticles (2–8 nm) are the active ones. Numerous approaches have been described in the literature to prepare such small gold nanoparticles on metal oxide supports, including incipient wetness impregnation, co-precipitation, deposition–precipitation, ion exchange, gas-phase grafting, co-sputtering, organic capping, and dendrimer and micelle encapsulation [13–23]. Among them, organic capping and encapsulation methods produce size-controlled gold nanopar-

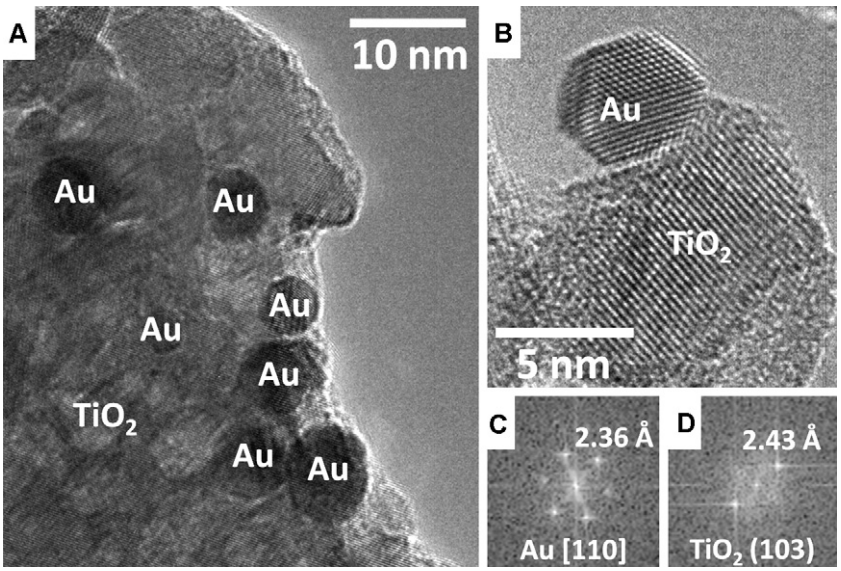

Fig. 3. (a) High resolution transmission electron microscopy (HRTEM) image of Au nanoparticles supported on TiO_2. (b) Detailed HRTEM image of an individual Au nanoparticle anchored on a TiO_2 crystallite. Their corresponding Fourier Transform images are shown in (c) and (d), respectively.

ticles whose particle size is established before deposition on the metal oxide support. Moreover, the coordinating ligands in the precursor solution and on the oxide surface prevent aggregation of the nanoparticles [24–27]. In this work, dendron encapsulated gold nanoparticles have been impregnated over the TiO_2 layer deposited on the microchannels of the silicon micromonoliths.

Fig. 2a shows a low-magnification transmission electron microscopy (TEM) image of the dendron encapsulated Au nanoparticles as prepared. The mean Au particle size is 2.5 ± 0.7 nm and the mean distance between neighboring particles is about 2.1 ± 0.9 nm, which corresponds well to the size of Au-dendron ensembles. Fig. 2b shows a high resolution transmission electron microscopy image (HRTEM) of several particles. In all cases Au nanoparticles are round-shaped and exhibit lattice fringes corresponding to Au (1 1 1) crystallographic planes at 2.35 Å, as measured in the Fourier Transform image (see inset). After impregnation of dendron encapsulated Au nanoparticles over TiO_2, silicon micromonoliths were calcined at 673 K in order to create catalytic active sites for CO-PrOx at the perimeter interface around Au nanoparticles [18]. As expected, Au nanoparticles increased in size due to the thermal treatment up to 5.1 ± 1.2 nm, but a narrow size distribution was maintained, as depicted in Fig. 3a. The interface between Au nanoparticles and the TiO_2 support crystallites is poorly defined and no epitaxial relationship exists. Such morphology is ascribed to highly defective areas, which are believed to favor highly active catalytic sites [18]. As an example, Fig. 3b shows a HRTEM image of an individual Au nanoparticle on top a TiO_2 crystallite showing poorly defined lattice fringes of the support at the metal-oxide

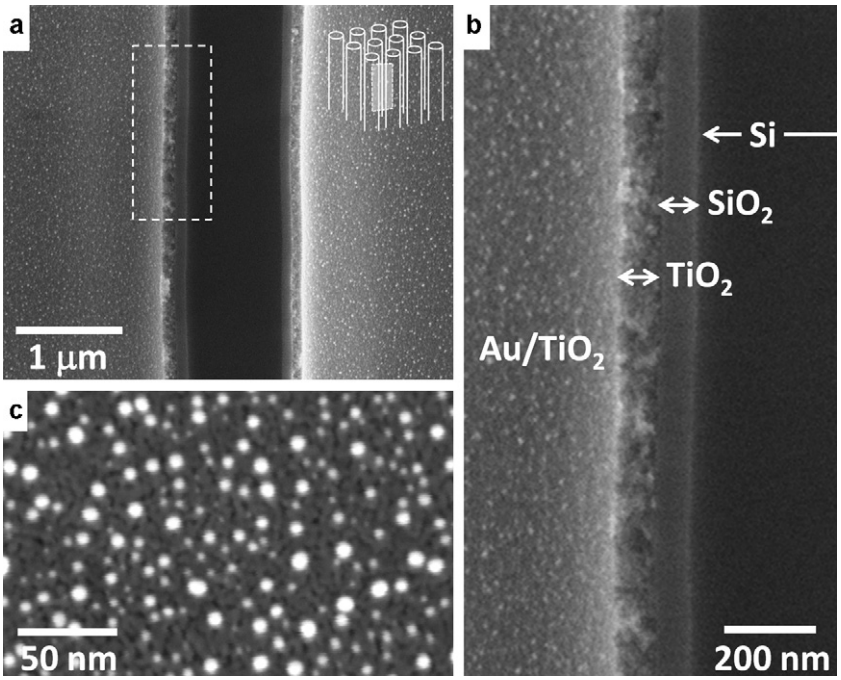

Fig. 4. Scanning electron microscopy (SEM) images of Au nanoparticles supported on TiO_2 over a SiO_2 layer grown onto a Si micromonolith ($Au/TiO_2/SiO_2/Si$). (a) Profile view along two adjacent channels close to the Si wall. (b) Enlarged area corresponding to the white square in (a). (c) High magnification image in planar view.

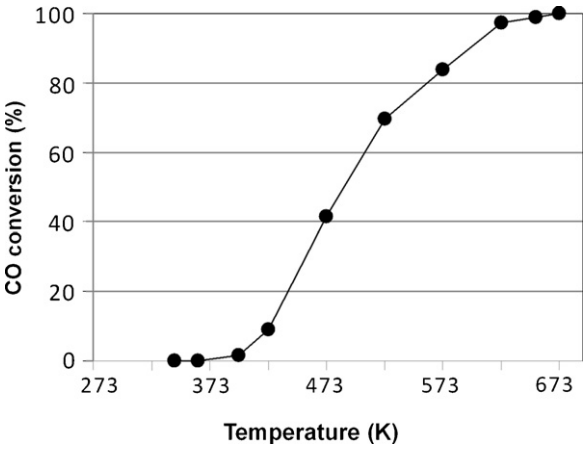

Fig. 5. CO oxidation over the Si micromonolith under $\lambda = 2$ and residence time of 90 ms.

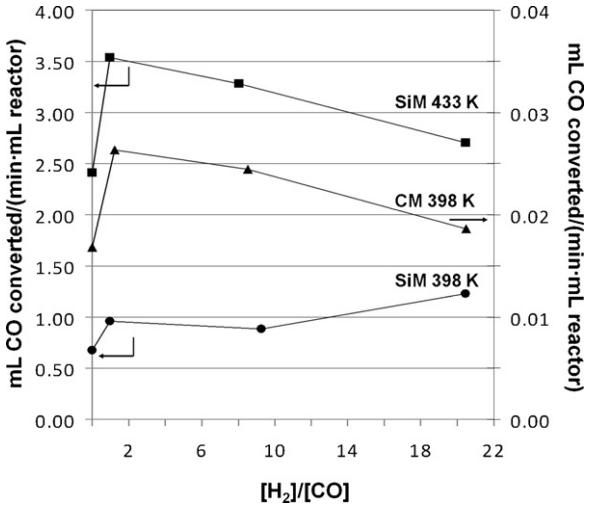

Fig. 6. CO oxidation activity normalized to the reactor volume under different H_2 concentration values. SiM = silicon micromonolith, CM = conventional monolith. $\lambda = 2$, residence times of 90 ms and 30 s for SiM and CM, respectively.

interface. From FT analysis it is deduced that the gold nanoparticle is oriented along the [1 1 0] crystallographic direction (Fig. 3c) over a TiO_2 crystallite showing (1 0 3) planes at 2.43 Å (Fig. 3d). The removal of the protecting dendrimer shell around gold nanoparticles was monitored by X-ray photoelectron spectroscopy (XPS). Several spectra were recorded in situ at increasing temperature in the range 398–723 K. The surface atomic ratio Au/C increased progressively up to 673 K, indicating loss of dendrimer shell; however, at 723 K the surface atomic amount of Au decreased, suggesting that at this temperature sintering of gold nanoparticles occurred. Therefore, the calcination temperature of 673 K seems the most appropriate for creating an active Au–TiO_2 interface while preventing Au aggregation. In all cases, the binding energies of Au 4d electrons recorded at 334.8 and 352.8 eV indicated that gold exists in a zero valence state [18,24].

Fig. 4 corresponds to scanning electron microscopy (SEM) images obtained directly on the resulting silicon micromonolith treated and functionalized with the method described and discussed above. A general profile view of two adjacent microchannels after cutting the micromonolith is shown in Fig. 4a, and a detailed image at higher magnification corresponding to the area enclosed by the white square in Fig. 4a is depicted in Fig. 4b. The dark area corresponds to the silicon matrix, which is covered by a compact, homogeneous, and well-defined SiO_2 layer of about 60 nm thick (dark grey). Over the SiO_2 layer a homogeneous, less compact, and very uniform layer of TiO_2 is perfectly anchored (light grey), which is about 80 nm thick. Au nanoparticles appear as bright and rounded dots over TiO_2; they are very well dispersed over the support (Fig. 4c). Therefore, here we have provided a well established methodology for coating silicon microchannels with a few micrometers in diameter with a thin layer of an Au/TiO_2/SiO_2 catalyst, with a total thickness below 150 nm and without channel blocking. It should be highlighted that similar catalysts loaded with other metal nanoparticles can be prepared by this method, opening the possibility of using such silicon micromonoliths for a wide range of reactions at the microscale.

3.2. Reaction tests

To test for a proper activity of the functionalized silicon micromonolith, a light-off curve of pure CO oxidation (equation 2) was conducted under a CO/air flow ($\lambda = 2$) diluted in Ar, maintaining a constant residence time of 90 ms. The results are reported in Fig. 5. We measured low CO conversions (<5%) in the usual range of operating temperatures for the CO-PrOx reaction over Au-catalysts ($T < 393$ K) and a light-off temperature (defined as T to reach 50% conversion) slightly above 473 K. Complete CO conversion ($y_{CO} < 5$ ppm as GC lower detection limit) was found for $T > 673$ K, which assures absence of both by-passes in the micromonolith-washer-casing assembly and channels without catalyst coverage.

$$CO + 1/2O_2 \rightarrow CO_2 \quad (2)$$

$$H_2 + 1/2O_2 \rightarrow H_2O \quad (3)$$

Functionalized silicon micromonoliths (SiM) as well as conventional monoliths (CM) were tested in CO preferential oxidation in the presence of hydrogen (which may undergo undesired oxidation as shown in equation 3). Samples were first activated under a CO:air:Ar = 2:11:101 molar mixture ($\lambda = 2$) at 473 K until steady-state was attained. This occurred after about 2 h on stream over the CM, where the CO conversion stabilized at 90%, and after ca. 4 h over the SiM, with a 45% of CO conversion. After activation, the temperature was lowered to 398 K, the steady-state CO conversions were measured and, afterwards, excess hydrogen was introduced in the reaction mixture at the expense of Ar to maintain a constant residence time of 30 s for the conventional monolith and 0.09 s for the silicon micromonolith. The ratio H_2 to CO was increased from 1:1 to 10:1 and to 20:1 and the reactor effluent was monitored by gas chromatography every 10 min for ca. 2 h at each condition. The same procedure was repeated at 433 K for the SiM in order to yield higher conversion at the low residence times at hand. No deactivation was detected after 83 h and 48 h of total operation for the SiM and the CM, respectively.

The direct comparison of performance between SiM and CM is unviable as the different dimensions of the supports prevent the use of the same operating conditions. In this context, we present in Fig. 6 for both monolith geometries the corresponding performances as specific activities, normalizing the amount of moles of CO converted per unit time with the reactor volume. The specific activities shown here correspond to CO conversions up to 25% for the SiM and 80% for the CM. For the operating conditions explored, higher temperatures render higher activities for the SiM. Operating at the same temperature level, the SiM shows an outstanding difference of specific activity of ca. 2 orders of magnitude higher when compared to the CM, although the conversion level of the SiM is lower than that of the CM. The increase in contact area from 2.8×10^3 to 3.5×10^5 m^2/m^3 as downscaling from the 400 cpsi cordierite monolith to the silicon micromonolith enhances the specific activity even when the reactor operates at lower residence time (ca. 330-fold lower). In terms of catalytic wall surface area, both reactor geome-

tries yield similar values (2.6–3.1 × 10^{-6} mol $CO_{converted}$ s^{-1} m^{-2} at 398 K and H_2/CO = 20), which demonstrates that contact area is the key parameter in catalytic performance.

Other remarkable effect for both monolith geometries is the enhancement in activity when hydrogen is added to the original CO/air/Ar feed mixture, probably due to the beneficial effect of water (formed by hydrogen oxidation), as reported elsewhere [28,29]. Conversely, for CO conversion levels above 20% (T = 433 K for SiM, T = 398 K for CM), higher amounts of hydrogen in the feed led to a progressive drop in specific activity (Fig. 6). For the CO-PrOx reaction, the selectivity is commonly defined as the ratio between the amount of oxygen used only for the CO oxidation and the total amount of O_2 reacted (CO and hydrogen oxidation, see equation 4). As widely known, the selectivity drops as the temperature increases [29,30]. We measured for the SiM under H_2/CO = 1 a selectivity drop from 70 to 61% when the temperature was increased from 398 to 433 K. The increase of H_2 concentration in the feed mixture also affected the selectivity negatively; for the SiM we measured at 433 K selectivities of 61, 53 and 42% for H_2/CO ratios of 1, 10 and 20, respectively.

$$\text{Selectivity} = \frac{\Delta \dot{n}_{O_2 \rightarrow CO_2}}{\Delta \dot{n}_{O_2 \rightarrow CO_2} + \Delta \dot{n}_{O_2 \rightarrow H_2O}} \quad (4)$$

An up-scaled design comprising several silicon micromonoliths in-series is being currently tested to explore the CO-PrOx reaction up to the CO conversion levels required for proper PEMFC operation.

4. Conclusions

An effective methodology for coating silicon microchannels with a thin, homogeneous, and well-adhered Au/TiO_2 catalyst layer has been developed. Reaction experiences have shown that Si micromonoliths loaded with Au/TiO_2 prove adequate to conduct CO preferential oxidation in the presence of high amounts of hydrogen. CO conversion up to 25% has been attained at 90 ms residence time and specific activity values normalized per reactor volume amount to about 2 orders of magnitude higher when compared to conventional 400 cpsi cordierite monoliths.

Acknowledgements

Financial support from MICINN projects CTQ2009-12520, TEC2008-02520 and CTQ2009-08795 is acknowledged. N.J.D. is grateful to UPC for a PhD grant. J.L. is grateful to ICREA Academia program.

References

[1] O. Korotkikh, R. Farrauto, Catal. Today 62 (2000) 249–254.
[2] G. Kolb, V. Hessel, V. Cominos, C. Hofmann, H. Löwe, G. Nikolaidis, R. Zapf, A. Ziogas, E.R. Delsman, M.H.J.M. de Croon, J.C. Schouten, O. de la Iglesia, R. Mallda, J. Santamaria, Catal. Today 120 (2007) 2–20.
[3] W. Ehrfeld, V. Hessel, H. Löwe, Microreactors—New Technology for Modern Chemistry, Wiley-VCH, Weinheim, 2000.
[4] G. Kolb, Fuel Processing for Fuel Cells, Wiley-VCH, Weinheim, 2008.
[5] J. Llorca, A. Casanovas, T. Trifonov, A. Rodríguez, R. Alcubilla, J. Catal. 255 (2008) 228–233.
[6] A. Casanovas, M. Domínguez, C. Ledesma, E. López, J. Llorca, Catal. Today 143 (2009) 32–37.
[7] H. Idriss, M. Scott, J. Llorca, S.C. Chan, W. Chiu, P.Y. Sheng, A. Yee, M.A. Blackford, S.J. Pas, A.J. Hill, F.M. Alamgir, R. Rettew, C. Petersburg, S. Senanayake, M.A. Barteau, ChemSusChem 1 (2008) 905–910.
[8] E. López, A. Irigoyen, T. Trifonov, A. Rodríguez, J. Llorca, Int. J. Hydrogen Energy 35 (2010) 3472–3479.
[9] M. Haruta, M. Daté, Appl. Catal. A 222 (2001) 427–437.
[10] V. Lehmann, H. Föll, J. Electrochem. Soc. 137 (1990) 653–659.
[11] M. Brust, M. Walker, D. Bethell, D. Schiffrin, R. Whyman, J. Chem. Soc. Chem. Commun. (1994) 801.
[12] F. González de Rivera, L.I. Rodríguez, O. Rossell, M. Seco, N.J. Divins, I. Casanova, J. Llorca, submitted for publication.
[13] M. Haruta, Gold Bull. 37 (2004) 27.
[14] T. Hayashi, K. Tanaka, M. Haruta, J. Catal. 178 (1998) 566.
[15] Q. Fu, H. Saltsburg, M. Flytzani-Stephanopoulos, Science 301 (2003) 935.
[16] C. Mohr, H. Hofmeister, J. Radnik, P. Claus, J. Am. Chem. Soc. 125 (2003) 1905.
[17] J. Llorca, A. Casanovas, M. Domínguez, I. Casanova, I. Angurell, M. Seco, O. Rossell, J. Nanopart. Res. 10 (2008) 537.
[18] J. Llorca, M. Domínguez, C. Ledesma, R.J. Chimentão, F. Medina, J. Sueiras, I. Angurell, M. Seco, O. Rossell, J. Catal. 258 (2008) 187–198.
[19] J. Chou, N.R. Franklin, S.-H. Baeck, T.F. Jaramillo, E.W. McFarland, Catal. Lett. 95 (2004) 107.
[20] R. Zanella, S. Giorgio, C.R. Henry, C. Louis, J. Phys. Chem. B 106 (2002) 7634.
[21] L.D. Menard, F. Xu, R.G. Nuzzo, J.C. Yang, J. Catal. 243 (2006) 64.
[22] K. Mallick, M.J. Witcomb, M.S. Scurrell, Appl. Catal. A Gen. 259 (2004) 163.
[23] J.-D. Grunwaldt, M. Maciejewski, O.S. Becker, P. Fabrizioli, A. Baiker, J. Catal. 186 (1999) 458.
[24] J. Chou, E.W. McFarland, Chem. Commun. (2004) 1648.
[25] A.C. Templeton, W.P. Wuelfing, R.W. Murray, Acc. Chem. Res. 33 (2000) 27.
[26] C.-J. Zhong, M.M. Maye, Adv. Mater. 13 (2001) 1507.
[27] M.M. Maye, J. Luo, L. Han, N.N. Kariuki, C.-J. Zhong, Gold Bull. 36 (2003) 75.
[28] M. Schubert, A. Venugopal, M. Kahlich, V. Plzak, R. Behm, J. Catal. 222 (2004) 32–40.
[29] E. López, G. Kolios, G. Eigenberger, Ind. Eng. Chem. Res. 25 (2005) 9659–9667.
[30] M. Kahlich, H. Gasteiger, R. Behm, J. Catal. 182 (1999) 430–440.